Two-Dimensional Bimetallic Selenium-Containing Metal-Organic Frameworks and Their Calcinated Derivatives as Electrocatalysts for Overall Water Splitting

Zhao-ting Shang,[1] Tang-ming Li,[1] Bing-qian Hu,[1] Min Liu,[1] Wang-ting Lu,[1*](✉) Fan Yu,[1,*](✉) Yun Zheng[2,3*](✉)

[1]Key Laboratory of Optoelectronic Chemical Materials and Devices of Ministry of Education, College of Optoelectronic Materials and Technology, Jianghan University, Wuhan 430056, China

[2]Institute of New Energy Materials and Engineering, School of Materials Science and Engineering, Fuzhou University, Fuzhou 350108, China

[3]Department of Chemical Engineering, University of Waterloo, 200 University Ave. W, Waterloo, Ontario N2L 3G1, Canada

Supporting Information

1. Experimental section

1.1 Electrode preparation

The catalyst ink was created by ultrasonically combining 5.0 mg of the as-prepared catalyst with 30 μL of NaOH on solution and 500 μL of ethanol solvent for 30 minutes to create the working electrode, a glassy carbon electrode (5.0 mm in diameter).The surface of a glassy carbon electrode with a 5.0 mm diameter was then loaded with 20.0 μ L of the produced catalyst ink using a micropipette. Finally, a thin catalyst layer was formed by allowing the ink to dry overnight at room temperature. The acquired samples were combined with 30 weight percent of carbon black (Cabot Vulcan XC72) to increase conductivity while maintaining the weight of the entire catalyst mixture. Approximately 0.672 mg cm^{-2} of catalyst are loaded onto the glassy carbon electrode. Linear sweep voltammetry was performed in 1 M KOH at a scan rate of 5 mV s^{-1}. All the polarization curves were iR-corrected. Electrochemical impedance spectroscopy (EIS) in the range of 100 kHz ~0.1 Hz was analyzed. The stability of the catalyst was tested by chronopotentiometry method at 10 mA cm^{-2}.

[1] E-mail：yufan0714@163.com, luwangting08@163.com, yunzheng@fzu.edu.cn

1.2 Synthesis of Materials

1.2.1 Synthesis of ***CoFe/Se-MOF-1h***: The pristine $Co_{0.6}Fe_{0.4}$-MOF had been immersed in the aqua solution of SeO_2 for 1 h. After the filtration, the solid samples had been washed with water for three times, and dried for using as electrachemical measurements.

1.2.2 Synthesis of ***CoFe/Se-MOF-3h***: The pristine $Co_{0.6}Fe_{0.4}$-MOF had been immersed in the aqua solution of SeO_2 for 3 h. After the filtration, the solid samples had been washed with water for three times, and dried for using as electrachemical measurements.

1.2.3 Synthesis of ***Co/Fe/S/Se-500***: The CoFe/Se-MOF-5h had been placed in the tubular furnace under N_2 atmosphere, and then heated at 500 ℃ for 2 h. The resulted product are directly used as electrachemical measurements.

1.2.4 Synthesis of ***CoFe-MOF-Se-1***: The precise synthesis method and reagent amount were the same as for $Co_{0.6}Fe_{0.4}$-MOF, with the exception that KSeCN (0.1 mmol) was employed in place of KSCN. A sparkling pink crystal was obtained after several days.

1.2.5 Synthesis of ***CoFe-MOF-Se-3***: The precise synthesis method and reagent amount were the same as for $Co_{0.6}Fe_{0.4}$-MOF, with the exception that KSeCN (0.4 mmol) was employed in place of KSCN. A sparkling pink crystal was obtained after several days.

1.3 Calculation of TOF values

The TOF were calculated as follows the equation:

$$TOF = \frac{JA}{2FM},$$

where J is the current density at a defined overpotential, A is the geometric surface area of the electrode, 2 denotes the number of electron transfers during HER, F is the Faraday constant, and M is the number of moles of the active electrocatalyst.

2. Characterizations

2.1 Structural analysis of 2D Co0.6Fe0.4-MOF precursors

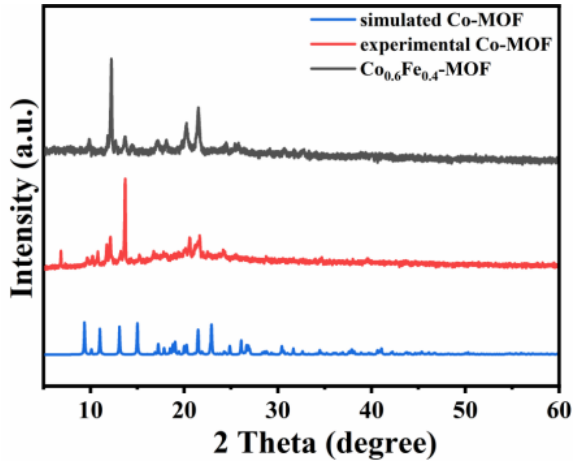

Fig S1. XRD pattern of as-prepared $Co_{0.6}Fe_{0.4}$-MOF, experimental Co-MOF and simulated Co-MOF.

Table S1. ICP-MS result of $Co_{0.6}Fe_{0.4}$-MOF

Sample name	Feeding molar ratio Co:Fe	Final molar ratio Co:Fe
$Co_{0.6}Fe_{0.4}$-MOF	0.6:0.4	0.56:0.44

Ref. S1. Han, J.; Hu, B.; Li, T.; Liang, H.; Yu, F.; Wang, L.; Zhao, Q.; Li, B., Modulating the Architectures of Cobalt Metal – Organic Frameworks to Fine-tune Slow Magnetic Relaxation Behaviors. *Crystal Growth & Design* **2021,** 21, (10), 5678-5686.

2.2 Structural analysis of CoFe/Se-MOF-1h, CoFe/Se-MOF-3h and CoFe/Se-MOF-5h

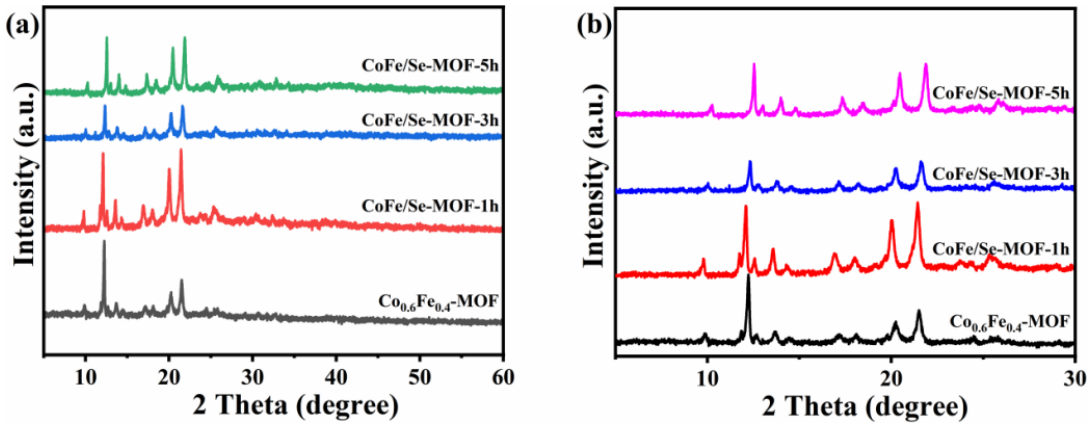

Fig.S2 (a) XRD patterns of $Co_{0.6}Fe_{0.4}$-MOF, CoFe/Se-MOF-1h, CoFe/Se-MOF-3h, and CoFe/Se-MOF-5h; (b) XRD spectrum partial enlargement.

2.3 Structural analysis of Co/Fe/S/Se-400 and Co/Fe/S/Se-500

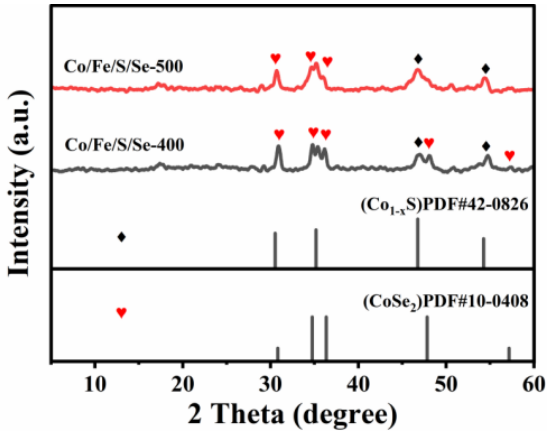

Fig.S3 XRD patterns of Co/Fe/S/Se-400 and Co/Fe/S/Se-500

2.4 Structural analysis of CoFe-MOF-Se-1、CoFe-MOF-Se-2 and CoFe-MOF-Se-3

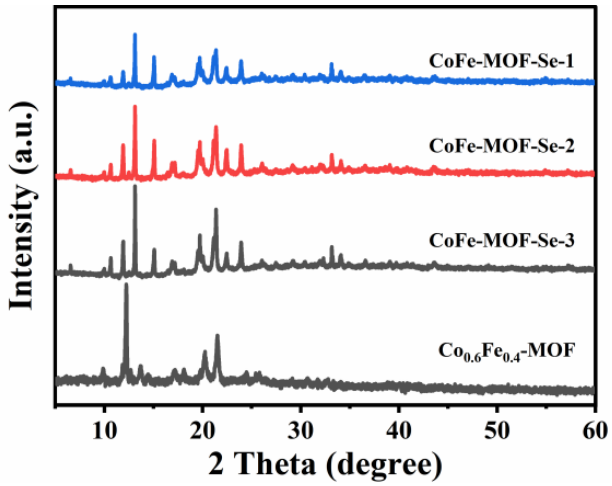

Fig.S4 XRD patterns of CoFe-MOF-Se-1、CoFe-MOF-Se-2 and CoFe-MOF-Se-3.

2.5 High resolution SEM and TEM of Co/Fe/S/Se-400 and Co/Fe/Se-400

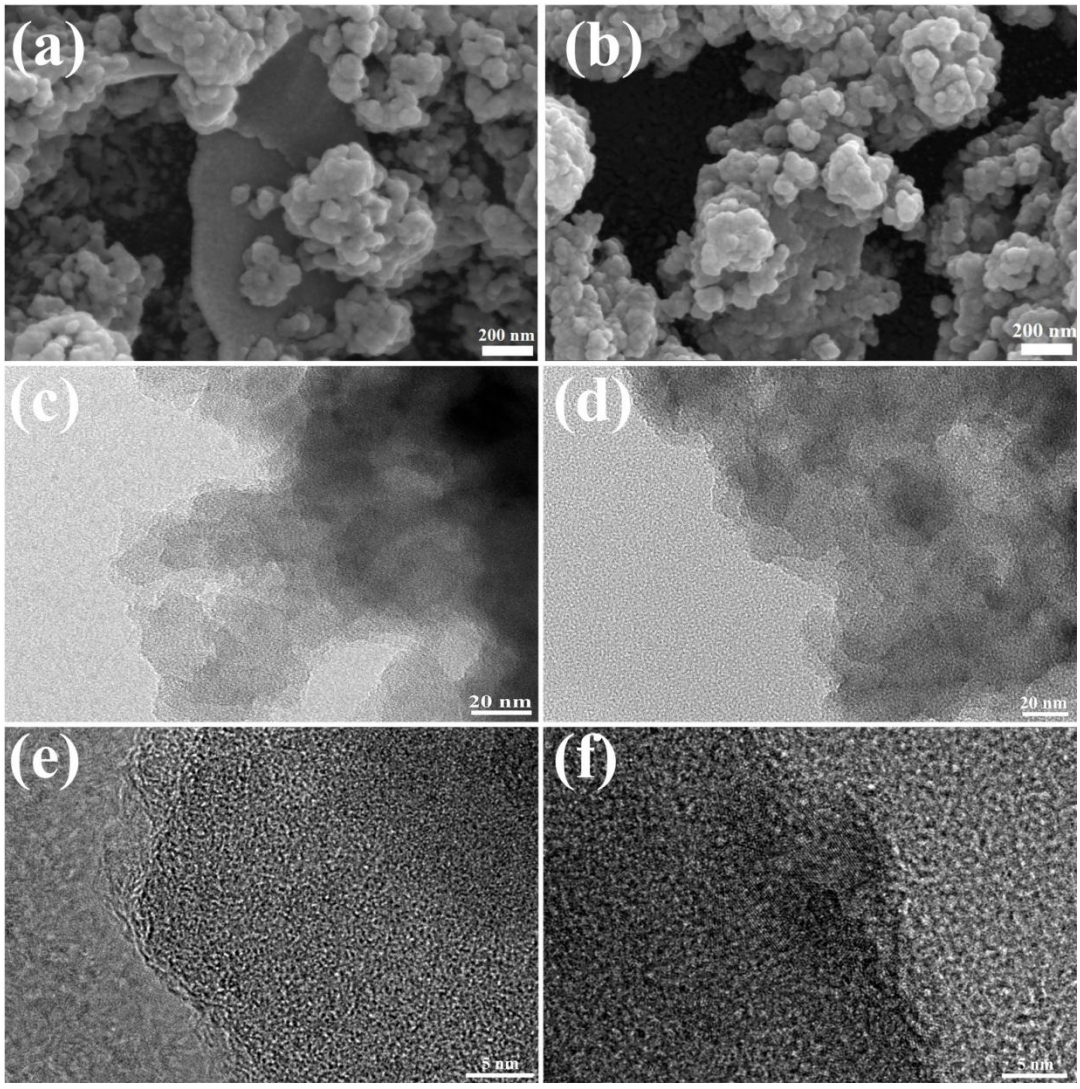

Fig.S5 SEM images for (a) Co/Fe/S/Se-400,(b) Co/Fe/Se-400 TEM images for (c,e) Co/Fe/S/Se-400,(d,f) Co/Fe/Se-400.

2.6 EDS mapping of characterization of CoFe/Se-MOF-5h, CoFe-MOF-Se, Co/Fe/S/Se-400 and Co/Fe/Se-400

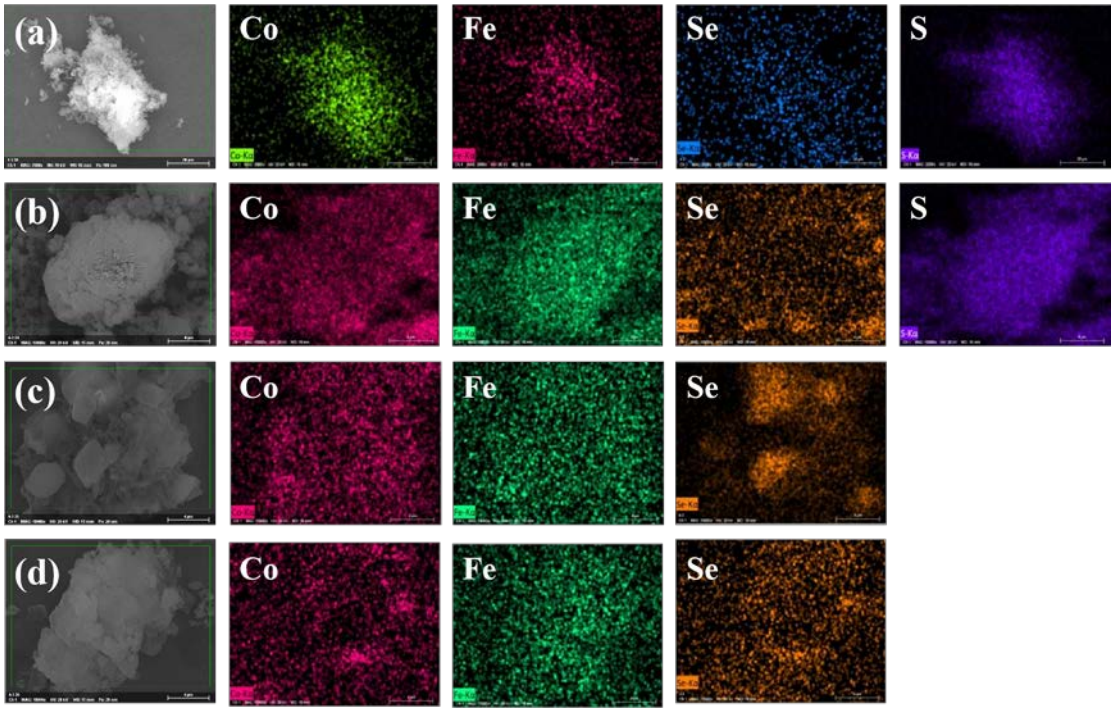

Fig. S6 EDS mapping of Co,Fe,Se and S (a) CoFe/Se-MOF-5h (b) Co/Fe/S/Se-400 ; EDS mapping of Co,Fe,Se (c) CoFe-MOF-Se (d) Co/Fe/Se-400.

2.7 BET surface areas of Co/Fe/S/Se-400 and Co/Fe/Se-400

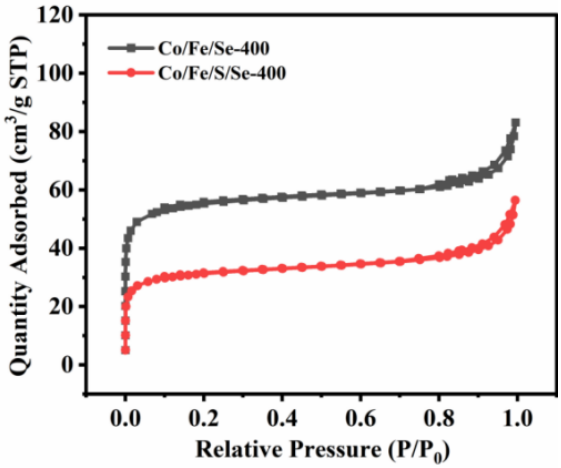

Fig. S7 N_2 adsorption-desorption isotherms of Co/Fe/Se-400 and Co/Fe/S/Se-400.

Table S2 Pore characteristics of Co/Fe/Se-400 and Co/Fe/S/Se-400

Samples	BET surface area (m^2/g)	Total pore volume (cm^3/g)	Average pore width (nm)
Co/Fe/Se-400	178.7207	0.127634	2.4079
Co/Fe/S/Se-400	102.4488	0.087215	2.7125

2.8 All XPS spectra of Co/Fe/S/Se-400, CoFe-MOF-Se, and Co/Fe/Se-400; (b-e) XPS spectra for Co, Fe, S, and Se in Co/Fe/S/Se-400

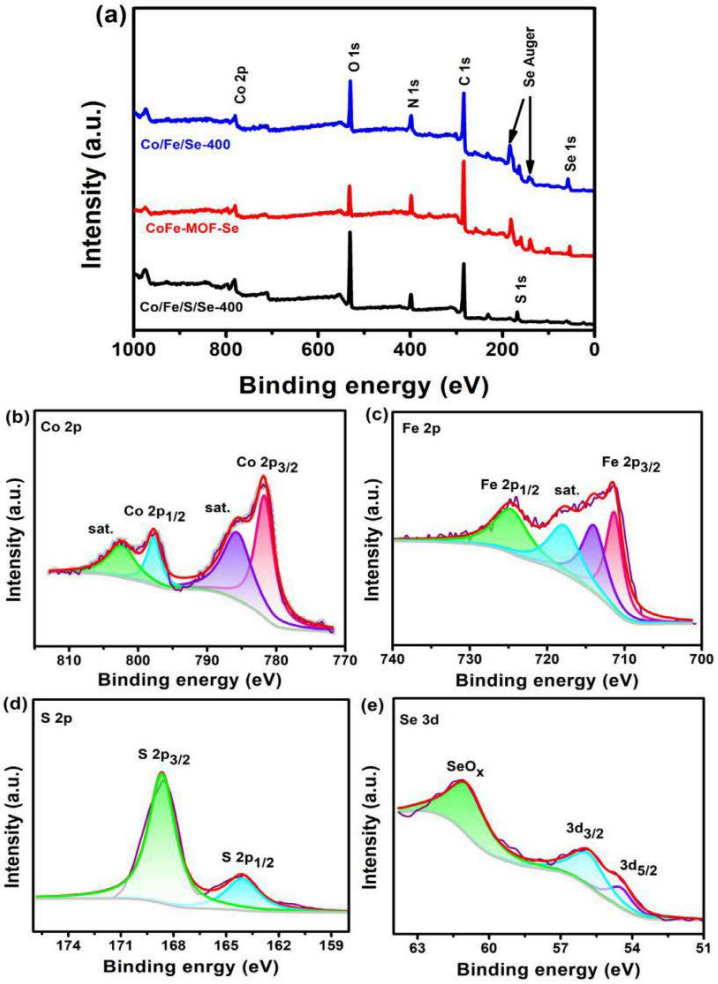

Fig.S8 (a) All XPS spectra of Co/Fe/S/Se-400, CoFe-MOF-Se, and Co/Fe/Se-400; (b-e) XPS spectra for Co, Fe, S, and Se in Co/Fe/S/Se-400.

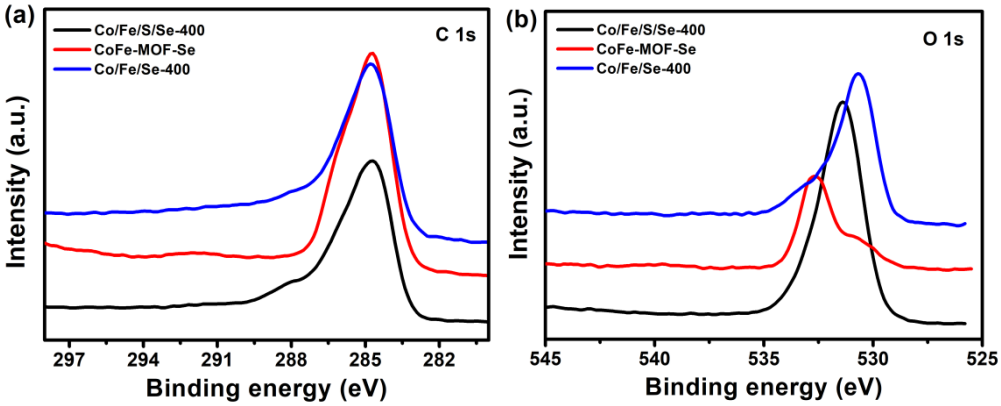

Fig. S9 XPS spectra of C (a) and O (b) in Co/Fe/S/Se-400, CoFe-MOF-Se, and Co/Fe/Se-400.

2.9 Electrocatalytic performances of CoFe/Se-MOF-1h, CoFe/Se-MOF-3h and CoFe/Se-MOF-5h

As shown in Fig. S5 (a-b). the overpotentials of $Co_{0.6}Fe_{0.4}$-MOF，CoFe/Se-MOF-1h, CoFe/Se-MOF-3h, and CoFe/Se-MOF-5h were 260, 271, 269, and 267 mV at 10 $mA \cdot cm^{-2}$, respectively. It can be seen that the etching time has little effect on the OER performance of bimetallic MOFs. As shown in Fig. S10(c-d), the overpotentials were 381, 316, 323, and 305 mV, respectively at 10 $mA \cdot cm^{-2}$. The comparison reveals that following SeO_2 etching, HER performances to some extent had been improved. When the etching time is 5 hours, the over potential of HER regulated by the etching time is the lowest, which could be due to the fact that as time passes, selenium becomes more complete, exposing more active sites, hence improving HER performance.

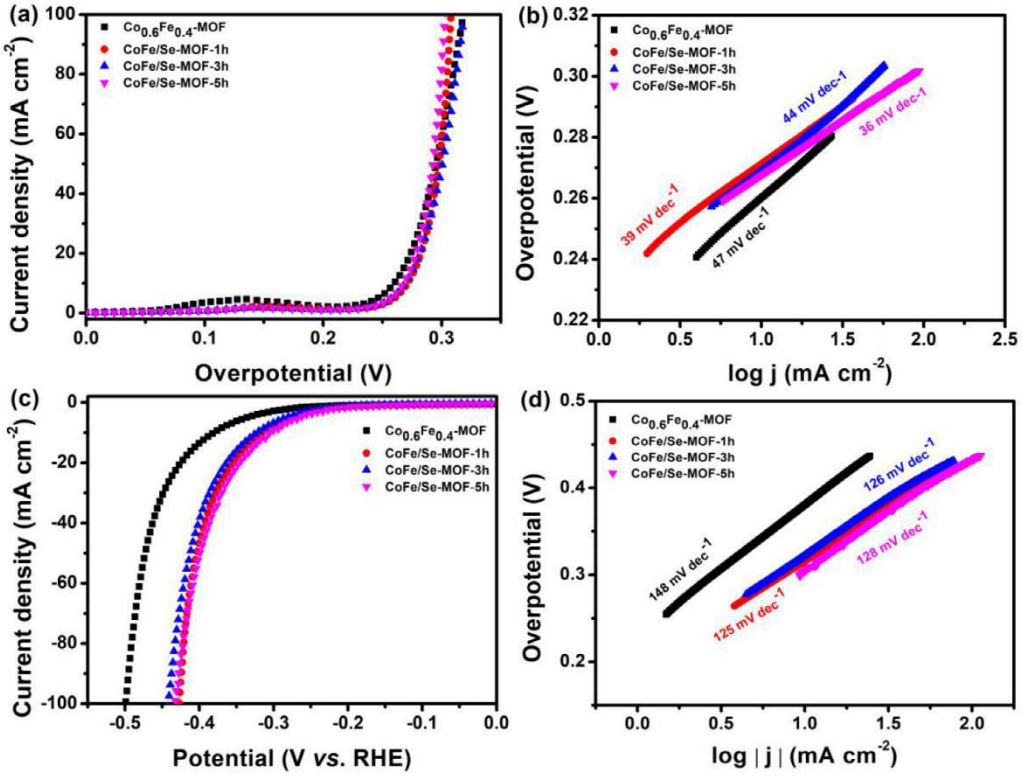

Fig. S10 LSV curves and Tafel curves of $Co_{0.6}Fe_{0.4}$-MOF, CoFe/Se-MOF-1h, CoFe/Se-MOF-3h and CoFe/Se-MOF-5h for (a-b) OER and (c-d) HER.

2.10 Electrocatalytic performances of Co/Fe/S/Se-400, and Co/Fe/S/Se-500

The OER polarization curve and Tafel slope of Co/Fe/S/Se-400 and Co/Fe/S/Se-500 are basically the same as $Co_{0.6}Fe_{0.4}$-MOF and CoFe/Se-MOF-5h, the overpotentials were both about 260 mV，as shown in Fig. S11(a-b). After SeO_2 etching and further

calcination at 400 and 500 ℃, little effect could be presented on the improvement of OER performance. The HER polarization curves of Co/Fe/S/Se-400 and Co/Fe/S/Se-500 show that the HER overpotentials are 225 and 254 mV, respectively at 10 mA·cm^{-2}, as shown in Fig. S11(c-d). It is easy to see from the results that the HER performance of the derived materials has been improved after high-temperature calcination, and the overpotential of Co/Fe/S/Se-400 is the smallest, indicating the calcination temperature of 400 °C is more favorable.

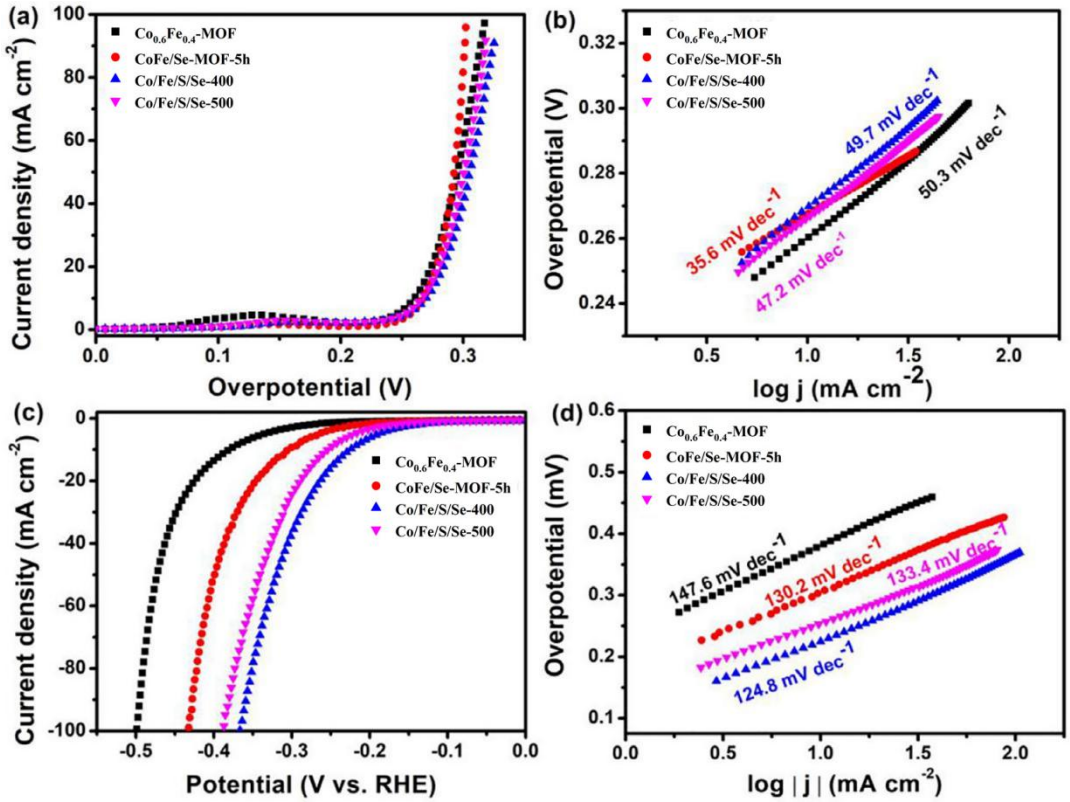

Fig. S11 LSV curves and Tafel curves of $Co_{0.6}Fe_{0.4}$-MOF, CoFe/Se-MOF-5h, Co/Fe/S/Se-400 and Co/Fe/S/Se-500 for (a-b) OER and (c-d) HER.

2.11 Electrocatalytic performances of CoFe-MOF-Se-1, CoFe-MOF-Se-2, CoFe-MOF-Se-3

The OER and HER polarization curve of CoFe-MOF-Se-1, CoFe-MOF-Se-2, CoFe-MOF-Se-3 are basically the same, as shown in Fig. S12(a-b). Little effect could be presented on the improvement of OER and HER performance.

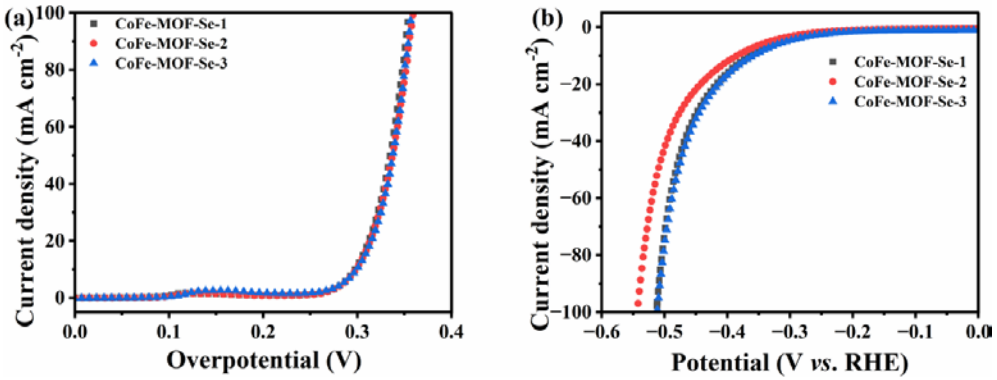

Fig. S12. LSV curves of CoFe-MOF-Se-1, CoFe-MOF-Se-2, CoFe-MOF-Se-3 for (a) OER and (b) HER.

Table S3. The related OER and HER parameters for $Co_{0.6}Fe_{0.4}$-MOF, CoFe-MOF-Se, Co/Fe/S/Se-400, and Co/Fe/Se-400

	Current density	$Co_{0.6}Fe_{0.4}$-MOF	CoFe-MOF-Se	Co/Fe/S/Se-400	Co/Fe/Se-400
	$mA \cdot cm^{-2}$	mV	mV	mV	mV
OER	10	260	300	273	270
	100	319	355	-	321
HER	10	381	360	225	235
	100	499	512	367	369

Table S4 Comparison between Co/Fe/Se-400 and other reported electrode materials

Material	Overpotential (HER)	Overpotential (OER)	Current density	Ref.
$FeSe_2$	244 mV	---	10 mA cm^{-2}	[67]
$CoSe_2$/C	253 mV	---	10 mA cm^{-2}	[68]
30% $FeSe_2$/GO	250 mV	---	9.68 mA cm^{-2}	[69]
$CoSe_2$-450	---	330 mV	10 mA cm^{-2}	[70]
$CoSe_2$-30	---	287 mV	10 mA cm^{-2}	[71]
6%Se-Co_3O_4	---	281 mV	10 mA cm^{-2}	[72]
$Co_{0.8}Fe_{0.2}Se_2$	---	345 mV	10 mA cm^{-2}	[73]
$CoSe_2$/CNTs	190 mV	300 mV	10 mA cm^{-2}	[74]
Co/Fe/Se-400	235 mV	270 mV	10 mA cm^{-2}	This work

2.12 Nyquist plots of different materials during HER

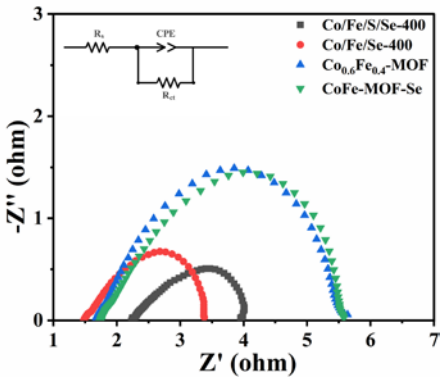

Fig. S13 Nyquist plots of different materials during HER

Table. S5 Values of R_s and R_{ct} of different materials during HER

	R_s	R_{ct}
Co/Fe/S/Se-400	2.276	1.979
Co/Fe/Se-400	1.526	1.876
$Co_{0.6}Fe_{0.4}$-MOF	1.668	5.393
CoFe-MOF-Se	1.714	3.936

2.13 SEM and TEM of Co/Fe/Se-400 and Co/Fe/S/Se-400 after cycling for HER and OER

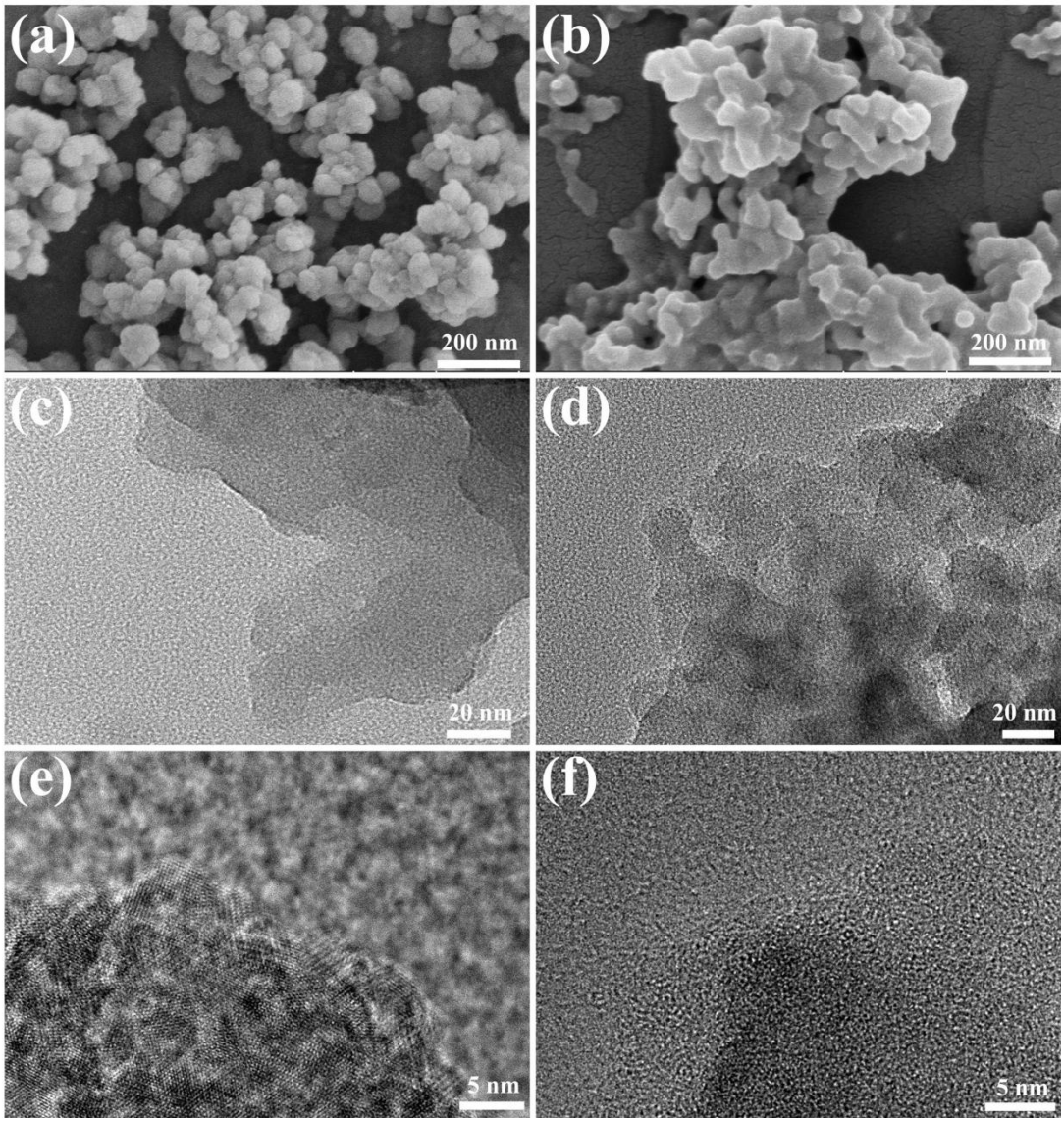

Fig. S14 SEM image after HER cycling for (a) Co/Fe/S/Se-400, (b)Co/Fe/Se-400 TEM images after HER cycling for (c,e) Co/Fe/S/Se-400,(d,f) Co/Fe/Se-400.

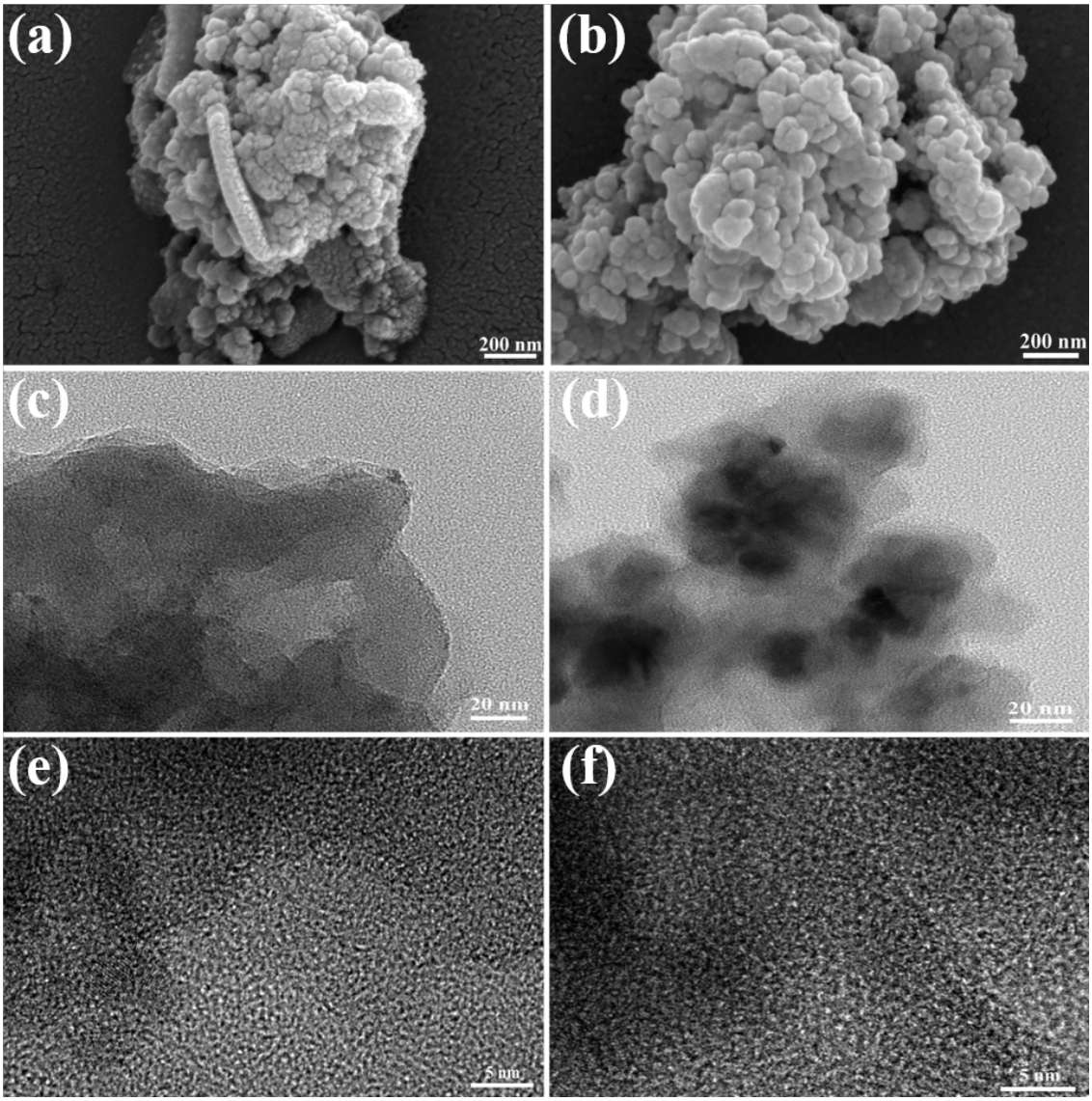

Fig. S15 SEM image after OER cycling for (a) Co/Fe/S/Se-400, (b)Co/Fe/Se-400 TEM images after OER cycling for (c,e) Co/Fe/S/Se-400,(d,f) Co/Fe/Se-400

2.14 XRD of Co/Fe/Se-400 and Co/Fe/S/Se-400 after cycling for HER

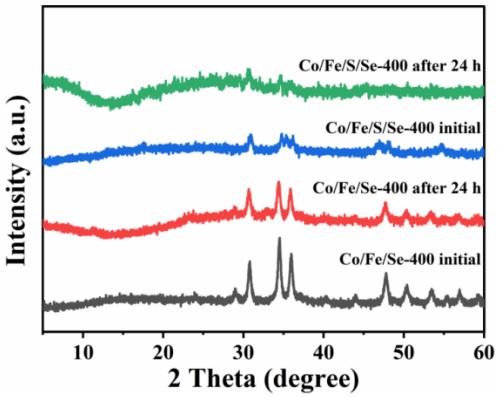

Fig. S16 XRD patterns of Co/Fe/S/Se-400 and Co/Fe/Se-400 initial and after cycling

for HER

2.15 The stability of Co/Fe/Se-400 and Co/Fe/S/Se-400 for OER

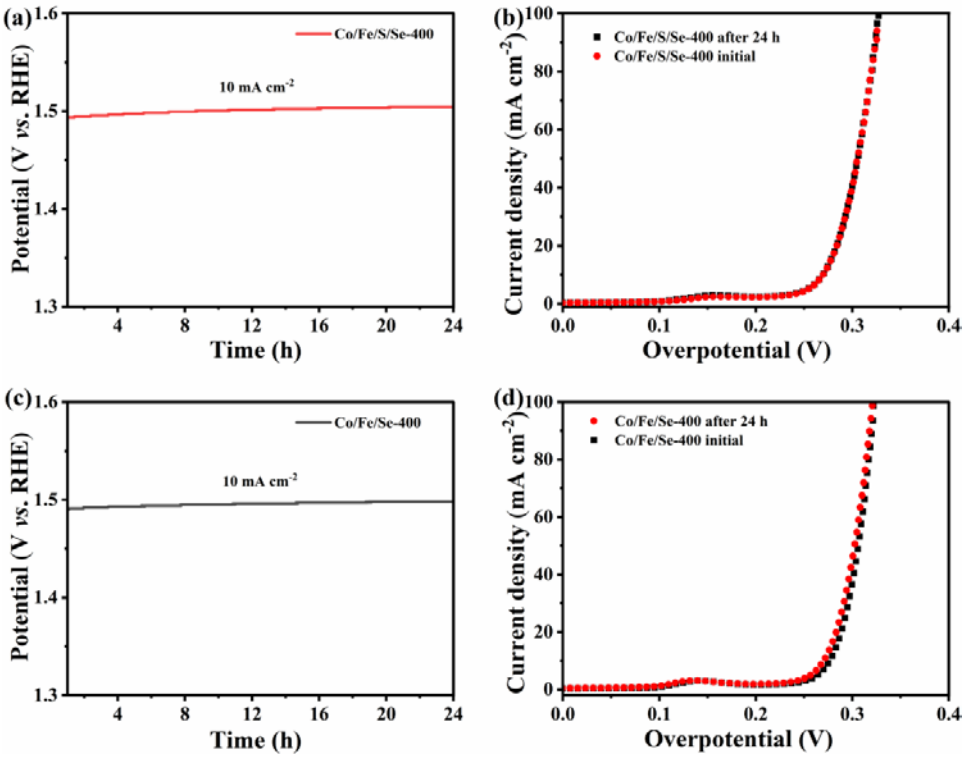

Fig. S17 OER time dependent curves at current density of 10 mA cm^{-2} (a) Co/Fe/S/Se-400 , (c) Co/Fe/Se-400; LSV curves of initial and after the measurements for OER (b)Co/Fe/S/Se-400 (d) Co/Fe/Se-400.